Particle–Surface Capillary Forces

ARTICLE *in* LANGMUIR · JUNE 1999

Impact Factor: 4.46 · DOI: 10.1021/la981095+ · Source: OAI

Particle−Surface Capillary Forces

A. de Lazzer, M. Dreyer,* and H. J. Rath

Center of Applied Space Technology and Microgravity, ZARM, Bremen University, Am Fallturm, 28359 Bremen, Germany

Received August 24, 1998. In Final Form: March 23, 1999

Particle−surface interactions due to capillary effects between spherical, paraboloidal, and conical particles and a flat substrate are considered. A recent approach given in a previous issue of *Langmuir* (Marmur, A. *Langmuir* **1993**, *9*, 1922) to obtain analytical estimates of the resulting capillary forces is discussed. Because Marmur's analytic approximation includes unnecessary simplifications, an improved formula for the approximation is given. Furthermore, the contribution of the surface tension forces acting along the contact line to the total adhesion force, which was deliberately omitted in the above cited work, is shown to be, in some cases, of similar order of magnitude as the capillary forces or even to exceed the latter. The range of applicability of the improved approach is verified by comparison with numerical solutions of the capillary equation for the liquid thread joining particle and substrate. The improved analytic approach is shown to be within ±5% of the exact solution for spherical and paraboloidal probes over a wide range of contact angles and contact line positions of the liquid bridge. However, for extreme configurations such as comparatively long and thin liquid bridges or when the absolute slopes of the interface at the contact lines on probe and surface differ greatly, large deviations might occur between approximation and the numerical solution. In such cases the numerical solution should be preferred to any approximation.

Introduction

Particle−particle and particle−surface or particle−substrate interactions in the presence of lubricating films are of considerable importance, for example in the study of partially wetted granular media and in the formation of liquid bridges under weightlessness conditions. They are also of importance for several measurement techniques among which are atomic force microscopy (AFM) and sphere or cone tensiometry. In the case of the measurement techniques, the correct interpretation of measurements depends heavily on the accurate determination of the liquid−solid adhesion forces caused by capillary action of the intermediate lubricating film. In this context, the total adhesion force can be divided into a "capillary force", originating from the capillary pressure difference across the curved surface, and an "interfacial tension force", originating from the surface tension acting tangentially to the interface along the contact line with the solid body.

In the present paper an analytic yet approximate approach for determining the contribution of the capillary forces to the total adhesion forces from the background of AFM measurements, which was originally published in this journal in 1993 (Marmur[1]) is discussed, modified, and compared with numerical solutions of the capillary equation. We improve the analytic approximate equation to determine the respective capillary adhesion forces between different shaped rotationally symmetric particles or probes (cone, paraboloid, and sphere) and a flat wall or substrate. Additionally, we include the interfacial tension force, which the liquid free surface along the contact line exerts on the probe. This is shown to reach the order of magnitude of the capillary forces. Following ref 1, the results of our modified approximation are compared with a simple classical approximation for the total adhesion force. To obtain a valid range of applicability, we compare our approximation with the actual total adhesion force as obtained from numerical simulations of the capillary interface between probe and substrate. The influence of the contact angles the liquid encloses with the probe and the substrate on the accuracy of the approximation is determined considering two cases: (i) when wetting conditions are the same on both probe and substrate and (ii) when they are different. It is shown that not only the probe−substrate separation but also the contact angles can generate substantial deviations between the approximation and the exact solution. The deviations of the approximate solution can be reduced by minimizing separation and choosing symmetric interface configurations, i.e., when the slopes of the interface at the contact points on the probe and substrate have similar absolute values and different signs. However, the issue of stability of the resulting liquid bridges shall not be discussed in this context. On this subject, we refer to refs 2 and 3.

Theory

Consider a particle or probe close to a flat solid wall with a small amount of liquid filling the gap, as depicted in Figure 1. We assume the problem to be symmetric with respect to the y-axis, thus the capillary surface joining the plate and the particle forms circular contact lines on both of them. To determine the adhesion forces exerted by the intermediate liquid volume, either the pressure within the liquid bridge or the curvature of its interface must be determined. In what follows, it is assumed that the influence of gravity g, characterized by the Bond-number $\mathrm{Bo} = \Delta\rho g L^2/\sigma$ is negligible, ($\mathrm{Bo} \ll 1$), where $\Delta\rho$ denotes the density difference across the free surface, σ is the surface tension, and L is a characteristic length. In the present case, where gravity most probably acts in positive or negative y-direction, the y-coordinate of the contact line on the probe y_p denotes an appropriate scaling coefficient.

* Corresponding author phone, +49 421-218-4038; fax, +49 421-218-2521; e-mail, dreyer@zarm.uni-bremen.de.

(1) Marmur, A. *Langmuir* **1993**, *9*, 1922.

(2) Schubert, H. *Kapillarität in porösen Feststoffsystemen*; Springer: Berlin, Heidelberg, New York, 1982.

(3) Myshkis, A. D.; Babskii, V. G.; Kopachevskii, N. D.; Slobozhanin, L. A.; Tyuptsov, A. D. *Low-gravity fluid mechanics: mathematical theory of capillary phenomena*; Springer: Berlin, Heidelberg, New York, 1987.

10.1021/la981095+ CCC: $18.00
Published on Web 05/14/1999

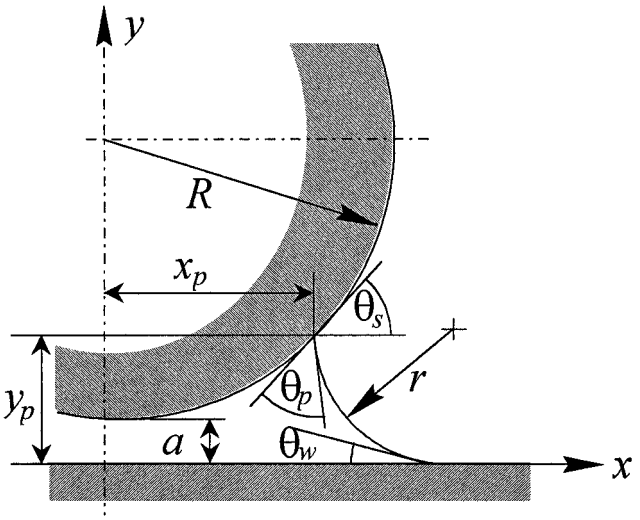

Figure 1. Geometry considered: liquid volume between a probe and a solid surface or wall. The configuration is rotationally symmetric with respect to the *y*-axis.

For vanishing Bond numbers, the actual shape of the interface is defined by Delaunay surfaces, the so-called unduloids and nodoids. They are described by boundary value problems of an ordinary first order differential equation which cannot be solved analytically; solutions can, however, be given in terms of elliptic integrals.[6,7] In any case, the unknown pressure within the fluid is the parameter to be adjusted, thus, exact solutions can only be determined by numerical means.

However, an approximation can be found when the free surfaces in a radial cross-section are assumed to have approximately circular shapes, as depicted above. Under this assumption, an analytical relation to determine the radius of curvature of the free surface can be derived. In a recent paper, Marmur[1] therefore referred to the center of the circular interface yielding a set of equations, which he assumed to have no analytical solution. On the basis of this premise, he introduced the additional simplifying approximation that the radii of the contact lines were almost identical and the related contact angles likewise. We will show that, by an appropriate choice of terms, an entirely analytic relation is obtained, which implies no restriction or assumption either on the position of the contact lines or on the contact angles.

Let r denote the unknown radius of curvature in a radial cross-section and θ_w and θ_p the contact angles that the liquid is supposed to form with the lower wall (or substrate) and the upper probe, respectively. Furthermore we introduce the slope of the probe's contour at the contact line θ_s (see Figure 1). Describing the contour of the probe with $y_p(x)$ and denoting derivatives with respect to x with a prime, θ_s is related to the slope of the interface $y'(x_p)$ at the contact line $(x_p, y(x_p))$ by $\theta_s = \arctan y'(x_p)$. From geometrical relations one obtains for the y-coordinate of the interface at the contact line that

$$y_p(x_p) = r\cos(\theta_p + \theta_s) + r\cos\theta_w \qquad (1)$$

yielding a completely analytic relation for the unknown radius of curvature that does not require any further simplifications

$$r = \frac{y_p(x_p)}{\cos[\theta_p + \arctan y'(x_p)] + \cos\theta_w} \qquad (2)$$

Using the Young−Laplace equation to determine the pressure drop across the interface and making the approximation that r and the radius of the contact line at the particle x_p are the principal radii of curvature of the interface in (x_p,y_p), the pressure difference across the free surface Δp becomes

$$\Delta p = \sigma\left(\frac{1}{x_p} - \frac{1}{r}\right) \qquad (3)$$

Here, positive and negative Δp correspond to repulsive and attractive forces on the probe, respectively.

The total adhesion force F between particle and substrate depends on the capillary adhesion due to the pressure difference across the free surface

$$F_A = -\pi x_p^2 \Delta p \qquad (4)$$

(with the sign changed to yield positive values in case of attraction or adhesion) *and* on the vertical component of the surface tension forces acting tangentially to the interface along the contact line

$$F_S = 2\pi x_p \sigma \sin(\theta_p + \theta_s) \qquad (5)$$

These yield together

$$F = F_A + F_S = -\pi x_p^2 \Delta p + 2\pi x_p \sigma \sin(\theta_p + \theta_s) \qquad (6)$$

It should be noted that in contrast to the adhesion force, which is subject to approximations, the contribution of the surface tension along the contact line according to eq 5 is mathematically exact. The contribution of the latter had nevertheless been deliberately omitted by Marmur.[1] We will show that it contributes significantly to the actual adhesion force. Using eqs 2 and 3 to express the pressure difference across the interface represents Marmur's so-called "numerical solution" which he considers in his conclusions to be preferable to the "symmetric case" (equal contact line radii) approximation. As his numerical solution is in fact analytical as shown above, we will refer to eqs 2 and 3 in conjunction with eq 6 in the following as the "approximate solution". The term numerical solution is used to denote solutions obtained by numerical integration of the Gauss−Laplace equation of the free surface, where the actual shape of the interface is considered. In the following, coordinates of the contact line will always refer to the probe's geometry. Thus the previous subscript for x and y is dropped and a new subscript for y, F, and θ_s is introduced that denotes the respective geometry of the probe (sphere, paraboloid, or cone).

Results and Discussion

Ratio of Surface Tension Forces to Capillary Adhesion. The capillary adhesion forces are determined for three different probes at different distances from the flat plate: a sphere of radius R, a paraboloid giving the asymptotic shape of this sphere in the limit of $x \to 0$ and a rectangular cone. The scaled distance of the apex of each probe from the substrate is denoted with a/R.

(4) Visser, J. In *Surface and Colloid Science*; Matjevic, E., Ed.; John Wiley & Sons: New York, 1976; Vol. 8, p 3.
(5) McFarlane, J. S.; Tabor, D. *Proc. R. Soc. London, Ser. A* **1950**, *202*, 224.
(6) Orr, F. M.; Scriven, L. E.; Rivas, A. P. *J. Fluid Mech.* **1975**, *67*, 723.
(7) Langbein, D. *Microgravity Sci. Technol.* **1992**, *5*, 2.

To quantify the contribution of the surface tension force along the contact line, the ratio ξ of surface tension forces F_S to capillary adhesion forces F_A is considered. Using eqs 4 and 5 one obtains

$$\xi = \frac{F_S}{F_A} = \frac{2\sin(\theta_p + \theta_s)}{\left(\frac{x}{r} - 1\right)} \tag{7}$$

This ratio will be discussed for the spherical, paraboloidal and conical probe.

The shape of the sphere $y_s(x)$ with radius R and distance a from the wall is given by

$$\frac{y_s}{R} = \frac{a}{R} + 1 - \sqrt{1 - \left(\frac{x}{R}\right)^2} \tag{8}$$

Inserting eq 8 into eq 2, the relative contribution of the surface tension along the contact line according to eq 7 becomes

$$\xi_s = \frac{2\sin(\theta_p + \theta_{s,s})}{\frac{x/R}{a/R + 1 - \sqrt{1 - (x/R)^2}}[\cos(\theta_p + \theta_{s,s}) + \cos\theta_w] - 1} \tag{9}$$

with

$$\theta_{s,s} = \arctan\left(\frac{(x/R)}{\sqrt{1 - (x/R)^2}}\right) \tag{10}$$

denoting the local slope of the sphere's contour.

For the paraboloid representing the asymptotic shape of the sphere for vanishing x/R, the shape of the probe is given by

$$\frac{y_p}{R} = \frac{a}{R} + \frac{1}{2}\left(\frac{x}{R}\right)^2 \tag{11}$$

and one obtains

$$\xi_p = \frac{2\sin(\theta_p + \theta_{s,p})}{\frac{x/R}{a/R + (x/R)^2/2}[\cos(\theta_p + \theta_{s,p}) + \cos\theta_w] - 1} \tag{12}$$

with

$$\theta_{s,p} = \arctan(x/R) \tag{13}$$

Considering finally the rectangular cone

$$\frac{y_c}{R} = \frac{a}{R} + \frac{x}{R} \tag{14}$$

and using $\theta_{s,c} = \arctan(1)$, the ratio of the surface tension forces to the capillary adhesion forces becomes

$$\xi_c = \frac{2\sin(\theta_p + \pi/4)}{\frac{x}{a + x}[\cos(\theta_p + \pi/4) + \cos\theta_w] - 1} \tag{15}$$

Obviously, the denominator of eqs 9, 12, and 15 might vanish eventually, yielding diverging ratios ξ. For convenience of plotting, we use the transformation $\Xi = \xi^{-1}/(1 + \xi^{-2})^{1/2}$ which maps the infinite range of possible ratios ξ ($-\infty < \xi < \infty$) onto the bounded interval $-2^{1/2} \le \Xi \le 2^{1/2}$. Thereby, $\xi = \pm 1$ is mapped to $\Xi = \pm 1$ and the range of configurations where the surface tension forces dominate $|\xi| > 1$ is mapped to $|\Xi| < 1$ with $|\Xi| \to 0$ for $|\xi| \to \infty$.

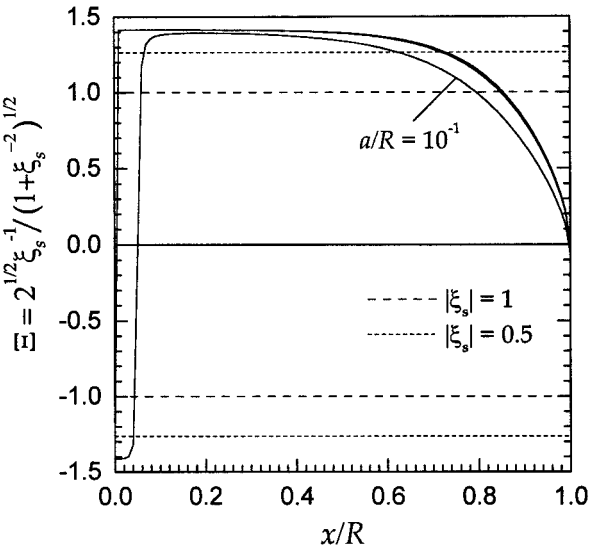

Figure 2. Mapped ratio ξ of surface tension forces along the contact line and capillary adhesion (approximation according to Marmur[1]) between a spherical probe and a flat surface; graphs for scaled distances $a/R = 10^{-1}, 10^{-2}...10^{-5}$ between probe and plate and contact angles $\theta_p = \theta_w = 0°$.

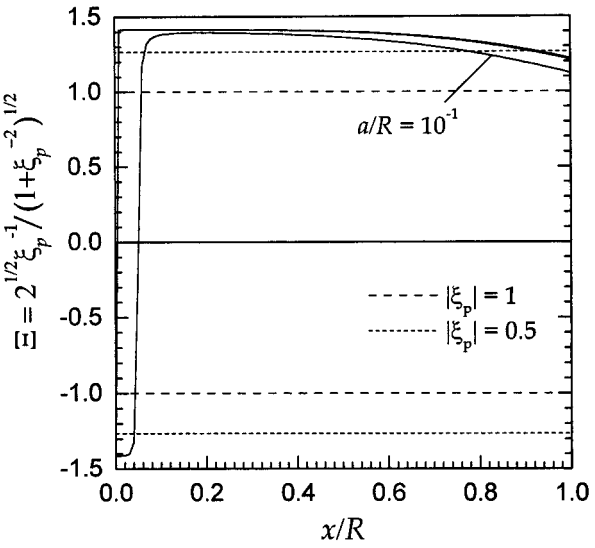

Figure 3. Similar to caption of Figure 2, for a paraboloidal probe.

For the geometries considered, the relative magnitude of the surface tension forces along the contact line of the probe compared to the capillary adhesion forces produced by the pressure jump across the free surface is depicted in Figures 2−4 in terms of Ξ for zero contact angles θ_p,θ_w. The ratios Ξ are determined as a function of the scaled local radius x/R of the probe and plotted for varying scaled distances $a/R = 10^{-1}, 10^{-2}...10^{-5}$ of the probe's tip from the solid wall. To facilitate interpretation of the plots, lines of constant Ξ corresponding to $|\xi| = 1$ ($F_S = \pm F_A$) and $\xi = 0.5$ ($F_S = \pm 0.5 F_A$) are added.

Obviously, the graphs tend toward a limiting curve for vanishing probe−substrate separations: in the case of sphere and paraboloid, the graphs for $a/R \le 10^{-2}$ cannot be distinguished, whereas for the cone, the respective graphs differ significantly only for $x/R \to 0$. The graphs of Ξ for the spherical and paraboloidal probes behave

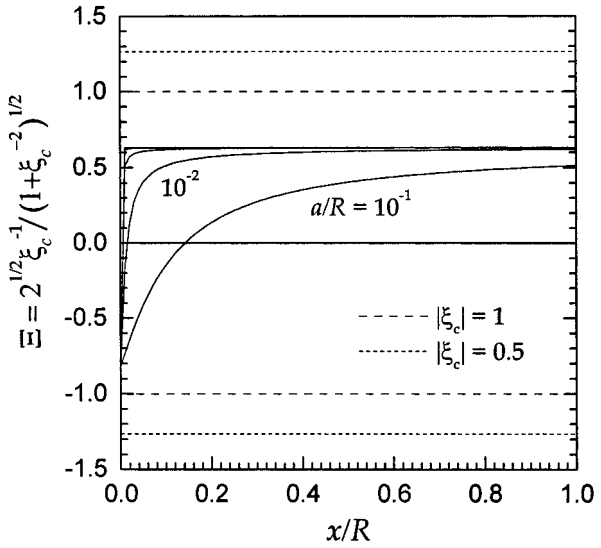

Figure 4. Similar to caption of Figure 2, for a conical probe.

fundamentally differently than those for the conical probes. While the former generally decrease with increasing x/R, which means that ξ is increasing, the latter approach a constant value. It should be stressed that the ratios ξ of the spherical probe diverge and change sign for any probe−substrate separation when $x/R \rightarrow 1$ is approached, although the corresponding zeros of Ξ are not resolved in our plots, because the denominator of eq 9 vanishes when $1 - x/R$ is of the order of $0.1\ (a/R)^2$.

From Figures 2−4 it follows that in the case of $\theta_p = \theta_w = 0°$ the contribution of the interfacial tension along the contact line to the total adhesion force might approach or even exceed the contribution of capillary adhesion for all probe geometries and all probe−substrate separations. For the conical probe, the contribution of the surface tension is always considerably greater than that of the capillary adhesion. Hereby one observes, that (i) for all probe geometries considered, Ξ decreases (i.e., ξ increases) with increasing probe−substrate separation a/R; and that (ii) with increasing x/R, Ξ decreases (i.e., ξ increases) for the spherical and paraboloidal probe, whereas for the conical geometry, Ξ and likewise ξ approach a constant value.

These observations lead to the conclusion that the aspect ratio of the liquid thread joining probe and substrate is a dominant factor influencing ξ. The latter (i) is directly related to the separation a/R and (ii) increases with x/R for the spherical and paraboloidal geometry. It remains almost constant or approaches a constant value when $x/R \gg a/R$ for the cone. Accordingly, because the y-coordinates of the paraboloid increase less rapidly with x/R than those of the sphere, so do the corresponding ratios ξ. In contrast, however, for the cone geometric similarity of aspect ratios is limited only by the magnitude of a/R compared to the size of the thread. For $x = O(a)$ the aspect ratio and its dependence on x is large and so is ξ and its variation, whereas for $x \gg a$ the aspect ratio and therefore ξ approaches a constant value.

To stress the importance of the aspect ratio of the liquid thread on ξ, selected interface configurations of the sphere, paraboloid, and cone yielding similar aspect ratios are compared. Because the respective geometries generate slopes of the probe's contour of different magnitude, no exact correspondence of the respective ξ can be expected. However, ξ can be expected to be of a similar order of magnitude. Thus, as sphere and cone approach similar y-coordinates and aspect ratios for $x/R \rightarrow 1$, the ratios ξ should behave similarly. Comparing the graphs in Figures 2 and 4 and accounting for the nonexistence of divergence in the case of the cone, it turns out that ξ is in fact of the same order of magnitude for both the sphere and the cone at $x/R \approx 0.95$. When comparing the sphere and paraboloid and omitting the influence of a/R, the aspect ratio of the paraboloid at $x/R = 1$ is similar to that of the sphere at $x/R \approx 0.8$. Consequently, the respective ratios Ξ should be of similar order of magnitude, too. This is confirmed by the graphs in Figures 2 and 3.

The results stress that the contribution of the surface tension forces along the contact line to the total adhesion forces is substantial. Their influence increases with the aspect ratio of the liquid thread. Furthermore, the influence of surface tension forces cannot be reduced to zero by reducing the aspect ratio, that is, by reducing the separation of probe and substrate. Owing to the inherent separation caused by the probe's contour, the ratio of surface tension forces to capillary adhesion forces approaches an asymptotic value for vanishing a/R. In the case of the cone, the latter is even associated with $\xi > 1$. Thus, when interpreting measurement data, one must account for the surface tension forces. Henceforth, in the following, the total adhesion forces, including both surface tension originated forces along the contact line and capillary adhesion due to the pressure difference across the interface, will be considered.

Comparison with Classical Approximation.[4,5] Although comparing one approximate solution with another cannot demonstrate the applicability of either of them, following Marmur[1] the results are initially compared with a classical but simple approximation[4,5] for the capillary adhesion force. When accounting for the influence of surface tension forces F_S along the contact line eq 5, this becomes

$$F^* = 4\pi R\sigma \cos\theta_p + 2\pi\sigma x_p \sin(\theta_p + \theta_s) \qquad (16)$$

Equation 16 is originally derived for spherical particles of radius R and is based upon the assumptions that the radius of the probe R is much larger than the radii of the contact lines on the two bodies involved, that the radii of the contact lines are equal, and that the distance of the particles is considerably smaller than the radius of the contact line.

Comparison of the different approximations is done in terms of the ratio F/F^* of total capillary adhesion forces according to eq 6, using the approximation eq 2 and the simple formula eq 16. Graphs for similar wetting conditions on probe and substrate with contact angles $\theta_p = \theta_w = 0°$ (solid lines), $\theta_p = \theta_w = 30°$ (dashed lines), and $\theta_p = \theta_w = 60°$ (dotted lines) are given in Figures 5−7 for scaled probe−plate separations of $a/R = 10^{-1}, 10^{-3}$, and 10^{-5}.

Similar to the behavior of Ξ, the graphs for constant contact angles approach a common envelope with decreasing probe−plate separation. Likewise, similar results are obtained for spherical and paraboloidal probes. Here, deviation of the capillary adhesion force according to the present approximation, eq 6, from the simple approach, eq 16, substantially increases with increasing contact angles. In contrast, the results for the conical probe show an entirely different behavior, with the contact angle having only weak influence on the scaled adhesion forces.

From Figures 5−7 it is obvious that the simple approximation of the capillary adhesion forces given in eq 16 is of no practical use when the approximation according to eq 6 is assumed to be at least more or less close to the actual adhesion force. The applicability of this assumption will be checked below, comparing our modified ap-

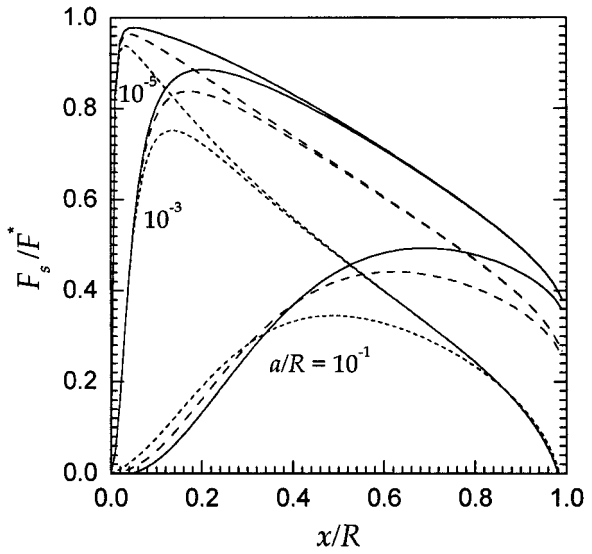

Figure 5. Scaled capillary adhesion force between a spherical probe and a flat surface for scaled distances $a/R = 10^{-1}$, 10^{-3}, and 10^{-5} of the probe from the plate and different contact angles $\theta_p = \theta_w = 0°$ (solid), $\theta_p = \theta_w = 30°$ (dashed), and $\theta_p = \theta_w = 60°$ (dotted).

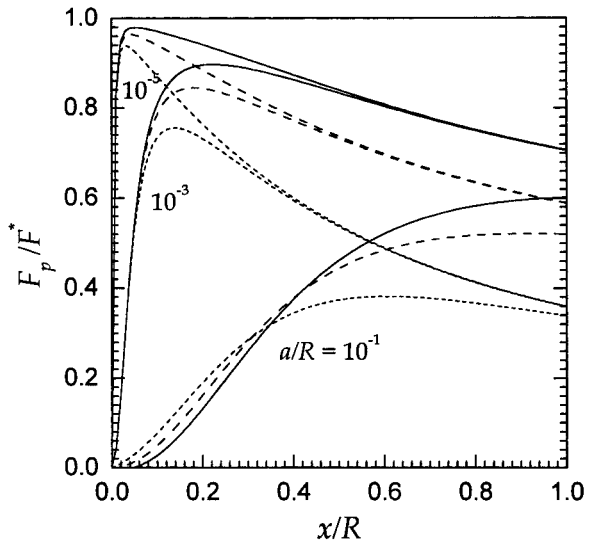

Figure 6. Similar to caption of Figure 5, for a paraboloidal probe.

proximation with the actual adhesion force obtained via numerical determination of the free surface properties. Furthermore, if an approximate solution of the capillary interface is to be applied and is to be compared with any solution of the total adhesion force, either approximate or numerical, the influence of surface tension along the contact line makes a substantial contribution and must be taken into account.

Comparison with Numerical Solution. The appropriateness of the circular interface approximation is considered in the following paragraph. The results for the total adhesion forces using the approximate equations 2 and 3 are compared with the actual total adhesion force as obtained from numerical determination of the mathematically exact curvature of the capillary interface by integrating the capillary equation of the free surface.

The capillary equation describing the free surface was solved numerically for vanishing Bond numbers to determine the actual pressure difference across the interface Δp and the actual adhesion force F in accordance with the assumptions above. The capillary equation was expressed

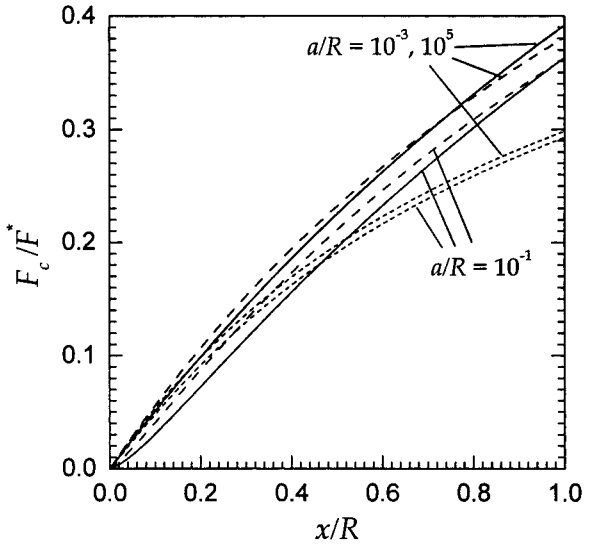

Figure 7. Similar to caption of Figure 5, for a conical probe.

in differential geometric terms for the curvature of a rotationally symmetric interface, yielding in cylindrical coordinates (see for example Myshkis et al.[3])

$$\frac{1}{x\sqrt{1+(\partial x/\partial y)^2}} - \frac{\partial^2 x/\partial y^2}{\sqrt{1+(\partial x/\partial y)^2}^3} = \frac{\Delta p}{\sigma} \qquad (17)$$

with x denoting radial and y axial direction as previously depicted in Figure 1. Alternatively, to avoid numerical problems due to diverging gradients $\partial x/\partial y$ when approaching the plate with zero contact angles, eq 17 can be expressed in terms of the inclination φ of the meniscus contour with respect to the positive x-axis and the arc length s of the interface. This yields the following system of coupled first-order differential equations[8]

$$\begin{aligned} \frac{\partial s}{\partial \varphi} &= \left(\frac{\sin(\varphi)}{x} - \frac{\Delta p}{\sigma}\right)^{-1} \\ \frac{\partial x}{\partial \varphi} &= -\cos(\varphi)\left(\frac{\sin(\varphi)}{x} - \frac{\Delta p}{\sigma}\right)^{-1} \\ \frac{\partial y}{\partial \varphi} &= -\sin(\varphi)\left(\frac{\sin(\varphi)}{x} - \frac{\Delta p}{\sigma}\right)^{-1} \end{aligned} \qquad (18)$$

Equations 17 and 18 denote boundary value problems and were solved iteratively using standard integration procedures (fourth or fifth order Runge−Kutta with adaptive stepping) to solve for the unknown pressure difference Δp. In the case of eq 17, the integration was carried out in the negative y-direction from the probe to the wall, starting at the probe with slope $\tan(\theta_p + \theta_s)$. Then Δp was adjusted to yield a slope of $-\tan\theta_w$ at $y = 0$. Similarly, in the case of eq 18, the integration was carried out with respect to φ, from $\theta_p = \theta_p + \theta_s$ at the probe to $\theta_p = 180° - \theta_w$ at the wall, and Δp was then adjusted to yield $y = 0$ at $\varphi = \varphi_p$. From the results of the numerical simulation, the adhesive forces F_A can be calculated by inserting the correct pressure difference Δp into eq 4. The actual total adhesion force F is then obtained straightforwardly by adding F_S.

To judge on the appropriateness of the approximation, the ratio of total capillary adhesion forces using the approximate relations eqs 2 and 3 to the adhesion forces

(8) Hartland, S.; Hartley, R. W. *Axisymmetric fluid-liquid interfaces*; Elsevier: Amsterdam, 1976.

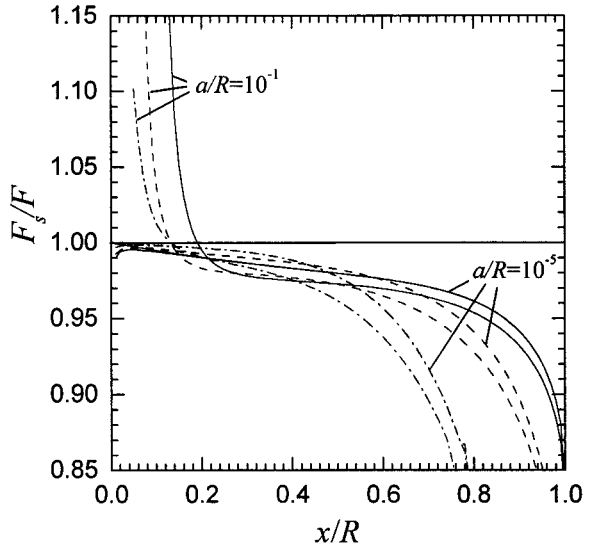

Figure 8. Accuracy of the approximate adhesion force with respect to the actual force F obtained from numerical determination of the interface for a spherical probe. Graphs for different contact angles $\theta_p = \theta_w = 0°$ (solid lines), 30° (dashed lines), and 60° (dash-dotted lines) and probe−plate separations $a/R = 10^{-1}$, 10^{-3}, and 10^{-5}. Except for vanishing x/R, the graphs for $a/R = 10^{-3}$ and 10^{-5} cannot be distinguished from one another for the contact angles considered.

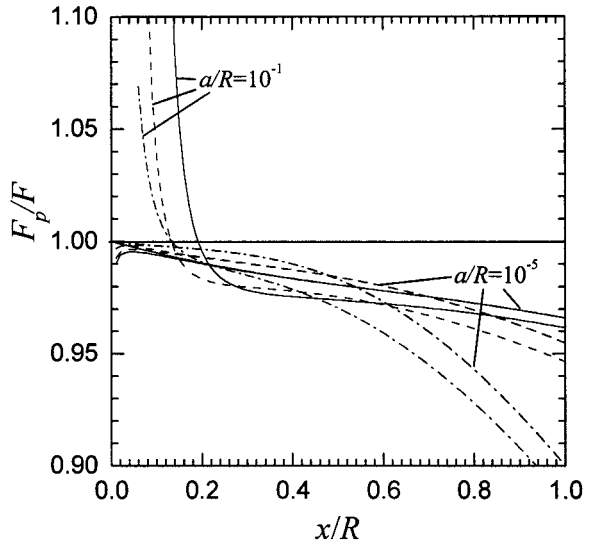

Figure 9. Similar to caption of Figure 8, for a paraboloidal probe.

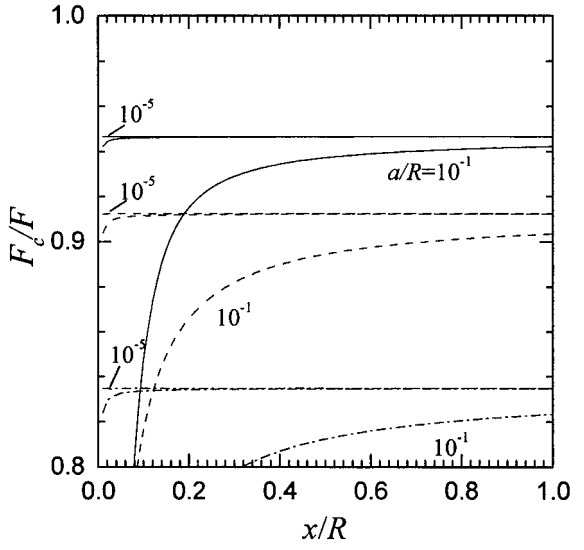

Figure 10. Similar to caption of Figure 8, for a conical probe.

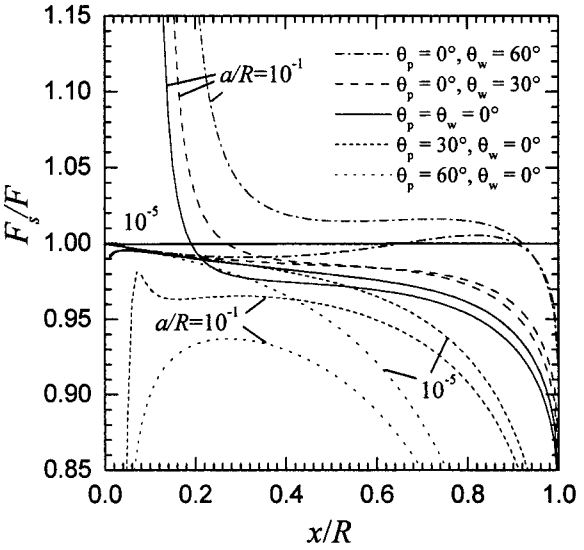

Figure 11. Accuracy of the approximate adhesion force for the spherical probe with respect to the actual force F for different contact angles and probe−plate separations $a/R = 10^{-1}$, 10^{-3}, and 10^{-5}. Except for vanishing x/R, the graphs for $a/R = 10^{-3}$ and 10^{-5} cannot be distinguished from one another for the contact angles considered.

from the numerical evaluation of the pressure difference across the interface is considered. In Figures 8−10, this ratio given for the different geometries of probe−plate separations $a/R = 10^{-1}$, 10^{-3}, and 10^{-5} with similar contact angles $\theta_p = \theta_w = 0°$, 30°, and 60° at the probe and at the wall. In Figures 11−13, this ratio is depicted for configurations showing different contact angles on the probe and substrate. The following series showing increasing contact angles at the probe and decreasing contact angles on the plate is considered: $\theta_p = 0° / \theta_w = 60°$, $\theta_p = 0° / \theta_w = 30°$, $\theta_p = \theta_w = 0°$, $\theta_p = 30° / \theta_w = 0°$, $\theta_p = 60° / \theta_w = 0°$. The graphs show that the solutions for $a/R = 10^{-3}$ and 10^{-5} largely coincide for all the contact angles and geometries considered. For the given resolution of the plots, deviations between these curves can be observed only in the limit of vanishing x/R.

From Figures 8, 9, 11, and 12 it can be observed that, for spherical and paraboloidal probes, the accuracy of the approximation with respect to contact angle and interface position on the probe is better than ±5% of the actual value for large ranges of interface positions x/R. The analytical relation using eqs 2 are 3 therefore gives a rather good estimate of the actual capillary adhesion forces for a wide range of applications with almost any separation of probe and substrate. However, considerable deviations are observed as $x/R \rightarrow 0$ and $x/R \rightarrow 1$, the deviations in the latter case increasing with increasing contact angles on the probe. In contrast, for the conical probe, the deviations of the approximate solutions from the numerical solutions are in most cases substantial and show only weak dependence on x/R when separations a/R are low. In a manner similar to the spherical and paraboloidal probes, the deviations increase with increasing contact angles.

A simultaneous increase of the contact angles on probe and plate improves the accuracy of the approximation at moderate x/R for spherical and paraboloidal probes. However, as already mentioned, for larger radial extensions of the liquid bridge, the approximation significantly underpredicts the actual adhesion force. Comparison of

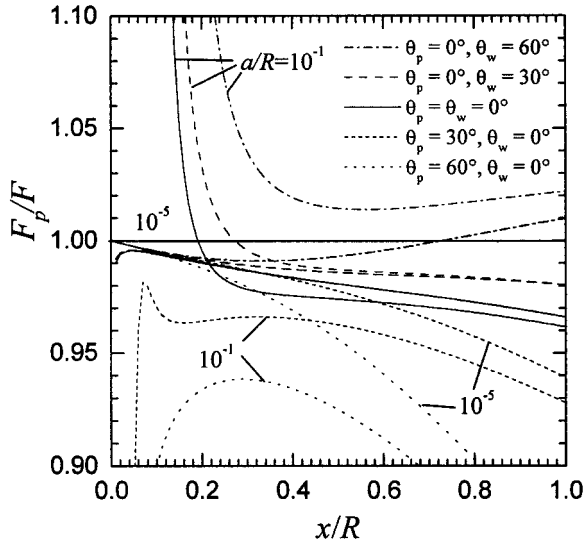

Figure 12. Similar to caption of Figure 11, for a paraboloidal probe.

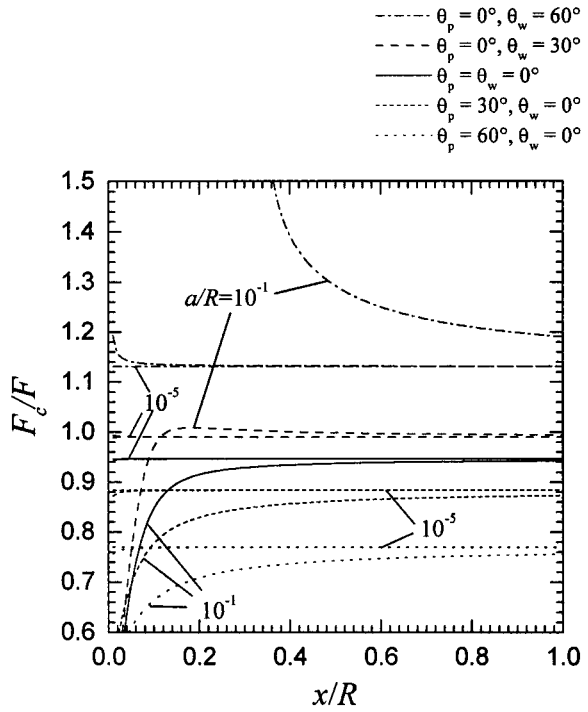

Figure 13. Similar to caption of Figure 11, for a conical probe.

the different graphs for the three probe geometries shows that the deviation depends predominantly on the actual slope of the probe. At the related radial coordinates for unit slope of the probe contour, $x/R \approx 0.7071$ and $x/R = 1$ for the spherical and paraboloidal probe, respectively, the scaled adhesion forces behave similarly to those of the rectangular cone (with constant unit slope).

When the liquid phase establishes different contact angles at the probe and the substrate, the accuracy of the approximate solution depends substantially on the degree of symmetry of the interface (see Figures 11−13). Large contact angles at the probe in conjunction with small ones at the substrate yield an increasingly asymmetric interface with respect to the slopes at the contact lines on the probe ($\theta_s + \theta_p$) and plate (θ_w), and the accuracy of the approximation significantly decreases for all but very small radial coordinates. On the other hand, if contact angles on the wall increase with the probe remaining completely wetted, the interface becomes more symmetric and accuracy is improved. The capillary adhesion force is eventually even overpredicted.

To explain this behavior, we consider two extreme configurations that arise for the spherical probe at separation $a/R = 10^{-1}$ (these are interfaces touching the probe at radial coordinates $x/R = 0.15$ and $x/R = 0.9$) and compare the actual nodoidal shape of the interface as obtained from the numerical integration of the boundary value problem eqs 17 and 18 with the approximate circular meniscus as depicted in Figure 14.

From the left sketch of Figure 14 the significant decrease of curvature of the nodoid with increasing radius is clearly visible. The figure illustrates a general characteristic of the approximation for interfaces with almost symmetric conditions, because it reveals that the curvature in a radial section of the approximation is always larger than the actual curvature. Because the concave curvature is related to a negative pressure difference, the approximation therefore yields exaggerated adhesive forces.

In this context, we should discuss the second radius of curvature, which in eq 3 was set equal to the radial coordinate. Mathematically, however, the direction of the principal radii of curvature at a given location of a surface is always given for both by the normal on the surface. That is, the actual second radius of curvature at the contact line is $x/\sin(\theta_p + \theta_s)$. Thus, the approximation overpredicts the second radius of curvature as well, unless the slope of the interface at the contact line of the probe is vertical. Because the second radius of curvature has opposite sign yielding a repulsive contribution to the capillary force, the errors in determination of the radii of curvature on the capillary force mutually compensate to some degree.

For the situation sketched in Figure 14 for small x/R, however, the curvature in the radial plane is overpredicted to an extent that cannot be compensated for by the overprediction of the second radius of curvature. In the example given, the approximated radius of curvature is about 0.055, whereas the actual curvature in the radial plane is about 0.09. The deviation in pressure, given by the difference in reciprocal values of radii cannot be compensated for by the reciprocal of $x/R = 0.15$. Furthermore, the partial compensation of errors means that using the actual second radius of curvature does not improve the approximation. In fact, for most x/R the graphs would be significantly shifted upward, lying further above the numerical solution than they are lying below when using eq 3, showing a steep descent to meet the actual approximation for vertical slopes of the interface at the contact line.

The situation is different for strongly asymmetric interfaces as depicted in the right-hand diagram of Figure 14. In this case, the approximation eq 2 underpredicts the actual curvature and thus the adhesive component of the capillary force. Since the second radius of curvature and the disjoining force are overpredicted as long as $\theta_p + \theta_s \leq 90°$, the adhesion according to the approximation is smaller than the actual value. This effect increases with the asymmetry of the interface. Thus, the decrease of the graphs for large x/R for both sphere and paraboloid can be explained. Between the extreme configurations, the characteristics change. From the graphs for the sphere and paraboloid in Figures 11 and 12 one can conclude that, especially for the paraboloid, an optimal pair of contact angles on the probe and substrate might exist, yielding almost perfect mutual compensation over almost the entire range of x/R. This is in fact remarkable, since the local slopes of the probe inevitably vary along x/R, meaning that the influence of the varying slope of the interface must be balanced by an accompanying change

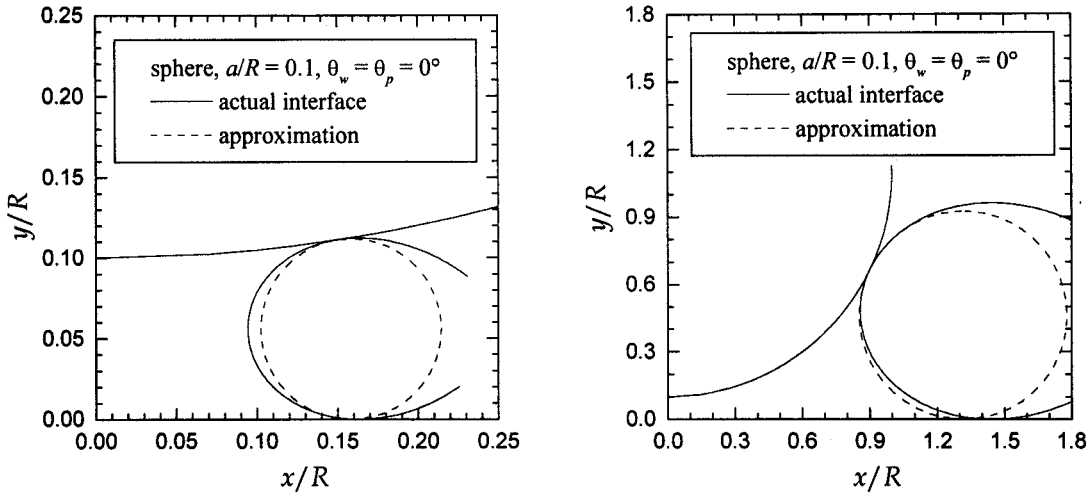

Figure 14. Comparison of actual capillary interface (nodoid) and the circular interface according to the approximate eq 2 for the interfaces touching the sphere at $x/R = 0.15$ (left) and 0.9 (right).

in aspect ratio. This is supported by the results for the conical probe. For small separations of the cone, both the aspect ratio of the liquid thread and the ratio of total adhesion forces is constant, with the former being independent of x/R. Therefore, the cone is able to produce an almost perfect compensation of the errors in the approximate equation by providing an appropriate interface geometry.

Conclusions

Considering the capillary adhesion forces between different shaped probes and a flat surface, an approximation for the latter was considered. This was based on the assumption of circular interfaces in a radial cross-section and was originally published in *Langmuir*.[1] In contrast to the previous work[1] that considered the equation to be nonanalytical, we have shown that an appropriate formulation renders an equation that can be solved analytically.

Because the approximation accounted only for the capillary forces due to the pressure difference across the free surface, the relative magnitude of surface tension forces along the contact line was studied. It was shown that for any probe geometry considered, the surface tension forces could reach the order of magnitude of the capillary forces or could even exceed them. Therefore, when considering adhesion forces in the context of measurements, the forces due to surface tension acting along the contact line cannot be neglected, i.e., the total capillary adhesion force accounting for both contributions must be regarded.

Following Marmur,[1] the total adhesion force according to the approximation was compared with a classical but very simple approach which was shown to yield unsatisfactory results for almost any condition possible.

To obtain a quantitative measure of the possible range of application of the approximation, the ratio of the total adhesion forces calculated according to the approximation to the exact adhesion force determined numerically by solving for the actual shape of the interface was considered. The accuracy of the approximation depends on the contact angles involved, the geometry of the probe, and the aspect ratio of the liquid thread or the radial coordinates. It was shown that for probe−plate separations below 10^{-3} their accuracy with respect to the exact solution is similar. For larger separations, however, the approximate solution becomes increasingly worse.

The accuracy is strongly influenced by the wetting conditions at the probe. Accuracy generally increases for symmetric interface configurations, i.e., when the slope of the interface at the contact line with the probe, inherently being bounded from below by the probe's shape, is compensated by the contact angle at the substrate exceeding the one at the probe. Because the results show almost constant deviations over substantial ranges of radial coordinates, it is concluded that the variation in aspect ratio of the liquid thread for the sphere and paraboloid favorably influences the results of the approximation. For conical probes with small separations $a/R \ll x$ the ratio of forces approaches a constant value for all radial coordinates when $a \ll x$.

In general, the deviation of the approximate solution from the exact value is less than 5% for a wide range of contact angles, probe−plate separations, and interface positions. However, for application in measurement techniques, the absolute value of the adhesion forces with respect to the forces to be measured must be taken into account. If the forces to be measured are small, as they usually will be in the context of AFM, the accuracy of the approximate solution might not be sufficient. Additionally, it should be taken into account that, depending on the wetting conditions, the accuracy of the approximation for small radial coordinates tends to diverge. Thus, deviations increase rapidly for small variations of contact line position. Similar effects can arise for large radial coordinates for the spherical and paraboloidal probe. In these cases, the numerical determination of the interface and its curvature is strongly recommended. For the conical probe, however, the approximate equation shows poor agreement with the actual adhesion force if the interface fails to exhibit almost identical absolute slopes at the contact lines.

Consequently, when interpreting experimental data in cases where capillary forces between probe and substrate due to a lubricating thread must be considered, the following approaches to optimize evaluation of these forces are suggested: (i) When a numerical simulation of each single measured configuration is not desired and when contact angles at the probe and substrate can be varied by an appropriate choice of materials or surface treatment, the accuracy of the approximation can be improved by increasing the contact angle on the substrate compared to the contact angle at the probe. (ii) When a numerical simulation of each single measured configuration is not

desired and contact angles cannot be varied, a paraboloidal probe should be preferred. The deviation of the approximation from the exact adhesion force is smaller for paraboloidal probes than for spherical or conical ones. (iii) However, when the actual forces to be measured are small compared to the capillary adhesion forces or when requirements on accuracy are high, a numerical determination of the capillary adhesion force cannot be avoided. In this case, one should account for the problem of defining appropriate contact angles between liquid and solid. Therefore, numerical fitting of the contour of the interface, e.g., to an image observed through a microscope, might yield better results than solving the differential equation of the interface where slopes and hence contact angles enter as boundary conditions. (iv) Alternatively, when a numerical simulation of each single measured configuration is not desired conical probes may be used. The cone enables the boundary conditions to be tuned on a way that produces an almost exact approximate solution. Furthermore, the cone provides the opportunity to obtain the appropriate scaling factor to calculate the actual adhesion force from the approximate solution by one single numerical solution of the capillary equation. Because the ratio of approximated and actual forces becomes constant for almost any x/R as long as a/R is small, the solution to the capillary equation considering the actual contact angles at probe and substrate for any x/R can be applied to other meniscus positions as well without a major lack of precision. Thus, since one single solution to the boundary value problem can be done even by trial and error, the cone provides the means to very accurately evaluating the total adhesion forces for any meniscus configuration at the least numerical expense.

Acknowledgment. Support by the German Aerospace Center (D.L.R.) under contract 50 WM 9432 is gratefully acknowledged.

LA981095+